euronoise

Tank experiments of sound propagation over a tilted bottom: Comparison with a 3-D PE model

Alexios Korakas[a], Frederic Sturm[a], Jean-Pierre Sessarego[b] and Didier Ferrand[c]

[a]Laboratoire de Mécanique des Fluides et d'Acoustique (UMR CNRS 5509), Ecole Centrale de Lyon, Centre acoustique, 36, avenue Guy de Collongue, 69134 Ecully Cedex, France
[b]Laboratory for Mechanics and Acoustics CNRS, 31 chemin Joseph Aiguier, 13009 Marseille, France
[c]Laboratoire de Mécanique et d'Acoustique (UPR CNRS 7051), 31, chemin Joseph Aiguier, 13402 Marseille Cedex 20, France
frederic.sturm@ec-lyon.fr

In this paper, we present results of laboratory scale experiments of long-range acoustic propagation over a wedge-shaped oceanic bottom. The present work comes as a continuation of the investigation of the wedge-like environment. Here, additional measurement campaigns are carried out. Received signals are recorded on a very fine spatial grid. During the experiment, a broadband source centered at 141.6 kHz was considered. Stacked time series *vs.* range and depth are displayed. In addition, transmission loss *vs.* range curves are extracted from time domain data, and exhibit remarkable 3-D effects. The purpose of this new series of experimental measurements is to collect high quality data to be inverted by means of matched field processing, where the replica will be provided by a fully three-dimensional parabolic equation code. Some technical issues involved in a model-based inversion using a 3-D code (*e.g.*, CPU time) are only discussed.

1 Introduction

Laboratory scale experiments provide control over the environmental parameters during the experiment and turn out to be a useful mean for testing 2-D or 3-D numerical propagation models in various scenarios [1]–[10]. The present work is part of a research program whose aim is to study the propagation of acoustic waves in well defined oceanic waveguides. The first step of this program was the calibration of the experimental facilities. It consisted in the investigation of shallow-water acoustic propagation in a Pekeris-like environment. Both continuous wave source [7] and broadband source pulses [10] were considered. The results were in rather good agreement with the predictions obtained using 2-D numerical models. However, it was pointed out that several combinations of water depth and bottom sound speed could lead to good agreement as well. The next step was a modification of the bathymetry in order to investigate more general 3-D waveguides. Preliminary experiments were carried out considering across-slope propagation over a wedge-shaped oceanic bottom. Non-negligible 3-D effects were observed and proved to compare favorably with numerical predictions obtained running a fully 3-D parabolic equation (PE) based code [9].

In the present work, additional series of experimental measurements of acoustic propagation in a wedge-like waveguide are performed. The signals are recorded on a very fine spatial grid. Only broadband pulse propagation is considered since transmission loss curves can be obtained at any desired frequency by means of appropriate Fourier transforms of time domain data, *cf.* [14]. In addition, broadband signals provide direct insight into the propagation features of the waveguide. They permit *in situ* preliminary tests for an optimal planification of the experimental procedure. The motivation for the planification is to obtain data that will be used in model-based inversions with replica provided by a fully 3-D PE code. In what follows, the experimental set-up is described and the experimental results are reported. Some technical aspects of an inversion procedure using a 3-D code are discussed.

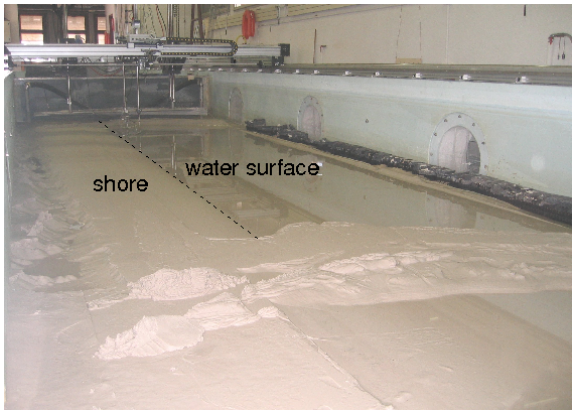

Figure 1: Shallow-water tank (facilities of the LMA-CNRS laboratory in Marseille, France).

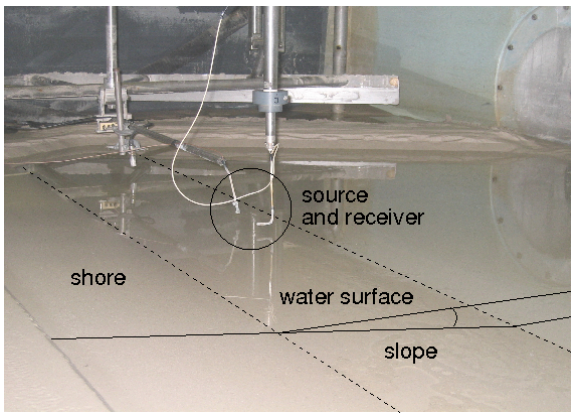

Figure 2: Wedge-like experimental configuration (with a slope of approximately 4.5°).

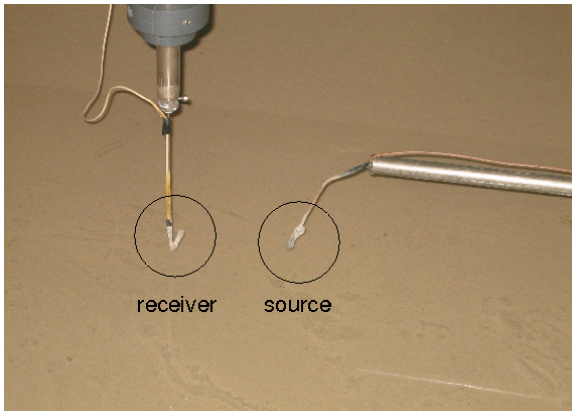

Figure 3: Source and receiver.

2 Experimental set-up

The experiments were carried out using the tank facilities of the LMA-CNRS laboratory in Marseille (France). The shallow water tank is 10-m-long and 3-m-wide, thus allowing for long-range propagation measurements, *cf.* Fig. 1. It contains a thin layer of water over a thick layer of calibrated sand simulating a bottom half-space. The grain size of the sand is considerably smaller than a wavelenght at the operational frequency. The set-up is

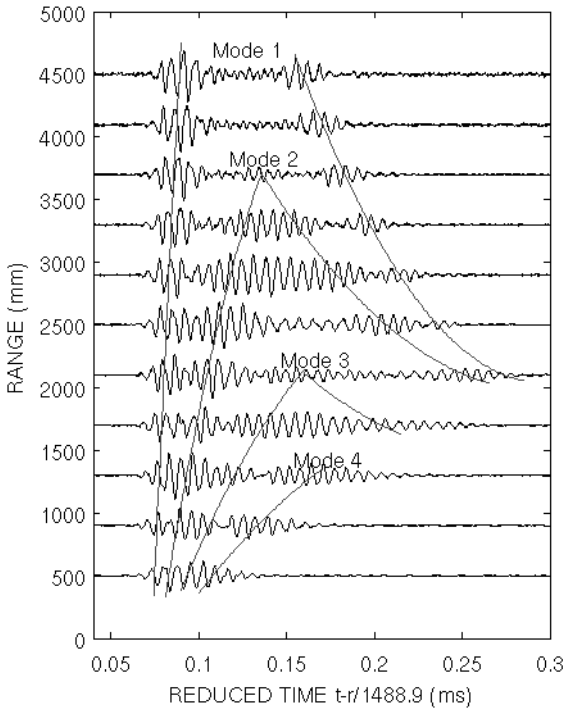

Figure 4: Stacked time series *vs.* source/receiver range. The source depth is 10 mm and the receiver depth is 10 mm. The lines superimposed on the time series indicate the evolution of the modes with range.

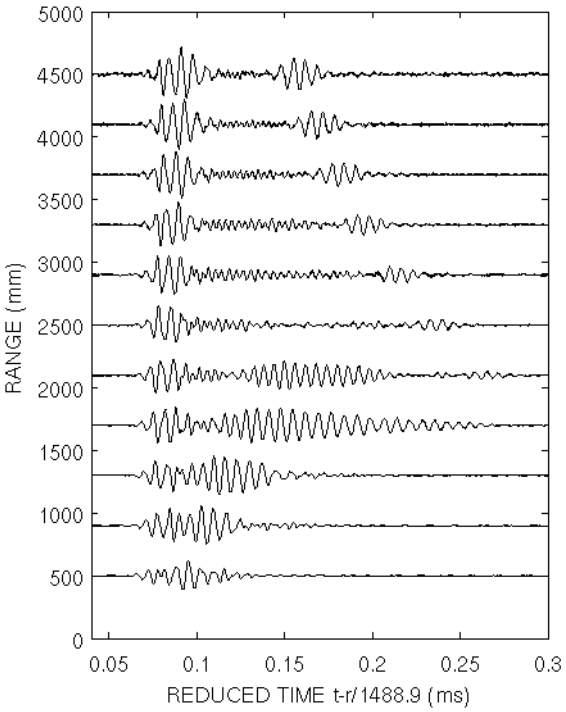

Figure 5: Stacked time series *vs.* source/receiver range. The receiver is now at a depth of 26 mm. Modes 2 and 4 almost vanish.

similar to the one described in [9]. It intends to simulate a shallow-water wedge-like environment. The bottom was tilted and made as flat as possible, *cf.* Fig. 2. The slope angle was approximately 4.5°. The source and receiver are cylindrical piezoelectric transducers both with diameters of 6.0 mm. They can been seen in Fig. 2 and a close-up is given in Fig. 3. The source can be positioned at any depth while the receiver is carried by a gantry allowing it to move in the three directions. During the measurement campaigns the source was fixed and the receiver moved within a vertical plane in the cross-slope (isobath) direction. More details about the experimental set-up can be found in [7] and [9].

3 Experimental results

3.1 Recorded time series

The source signal used was a broadband gaussian pulse centered at 141.6 kHz. The received signals were recorded along the cross-slope direction. For the measurement campaign presented here, the water depth at the source was 48 mm and the water sound speed was 1488.9 m/s (*cf.* [15]), leading to four propagating modes at the central frequency. The source was fixed at a depth of 10 mm. The signal was recorded at several source/receiver distances ranging from $r = 10$ mm to $r = 5000$ mm with increments of 100 mm, and at each range step it was recorded at depths between 1 mm and 45 mm with a depth increment of 1 mm. The results are presented in Figs. 4–8.

Figure 4 shows stacked time series *vs.* range at a receiver depth (RD) of 20 mm corresponding to no modal nodes. The data were scaled appropriately to compensate for geometrical spreading. The lines superimposed on the time series in Fig. 4 are drawn (approximately) to indicate the evolution of the initial pulse with range. We observe four modes undergoing strong 3-D effects. The modes are easily identified by inspection of the depth stacks at each specific range. For instance, they are shown in Figs. 6–8 at three distinct ranges. At short range the four propagating modes are present. Then, each mode, with the exception of mode 4 which appears to be very leaky compared to the others, present two distinct time arrivals at some specific range. For each mode, the temporal separation between these arrivals decreases with increasing source/receiver range. At a certain point, the multiple arrivals merge and the respective mode appears more dispersed. Farther in range, the wave packet corresponding to the merged arrivals of the same mode shortens, before being completely extinguished. The junction of the superimposed lines represent the approximate cut-off range for the relevant mode due to the 3-D mode shadowing effect. These effects are attributed to horizontal refraction of the acoustic energy. This behavior was predicted using a 3-D parabolic equation based code (see for instance in Ref. [12], where a detailed discussion can be found).

Figure 5 shows the same range stack at a receiver depth of 26 mm where modes 2 and 4 almost vanish. Modes 1 and 3 are now distinct even at short ranges and the multiple arrivals of mode 3 are clearly visible.

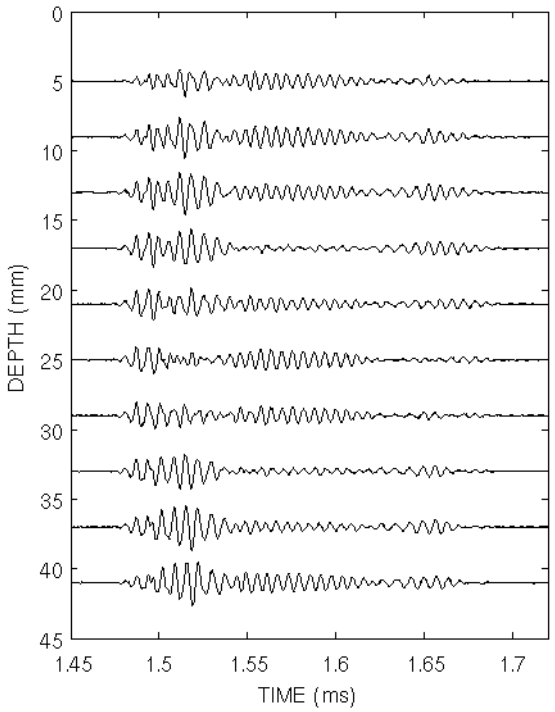

Figure 6: Stacked time series *vs.* receiver depth at a source/receiver range of 2100 mm. From left to right we identify mode 1, the first arrival of mode 2, two merged arrivals of mode 3, and a second arrival of mode 2.

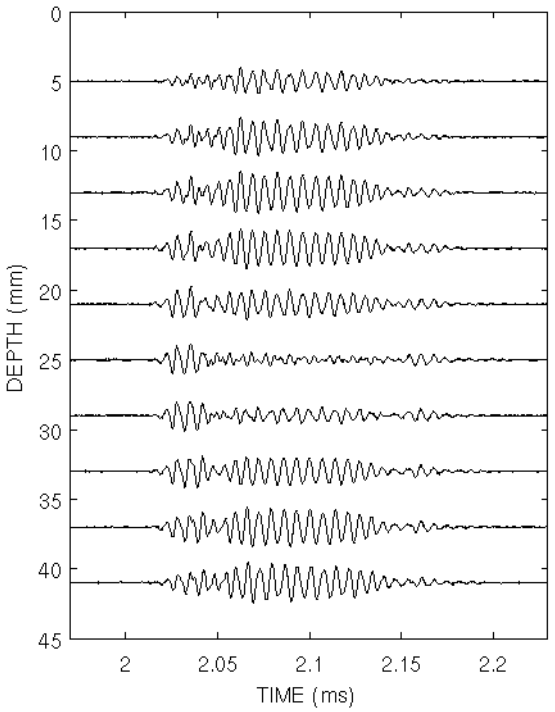

Figure 7: Stacked time series *vs.* receiver depth at a source/receiver range of 2900 mm. From left to right we identify mode 1, two merged arrivals of mode 2, and a second arrival of mode 1.

3.2 Transmission loss

Transmission loss data at any frequency within the bandwidth of the source signal is extracted by means of Fourier transform of the time series. To this end we use results from another measurement campaign that provide finer sampling in range. The water depth at the source was 48 mm and the water sound speed was 1488.6 m/s. Again four propagating modes are excited at the source. The receiver was fixed at a depth of 10 mm, and the signals were recorded for several source/receiver distances ranging from $r = 10$ mm to $r = 5000$ mm with increments of 5 mm. The experiment was repeated for three different source depths (SD):

- SD = 10 mm (all modes are excited),
- SD = 26.9 mm (modes 2 and 4 are weakly excited),
- SD = 19 mm (mode 3 is weakly excited).

In Fig. 9 we present transmission loss *vs.* range curves at three different frequencies for a source depth of 10 mm. The transmission loss patterns are similar in all three cases. However, as frequency increases, they are stretched out and shifted at higher ranges, as predicted in [11] and [13]. Note that the frequency 122 kHz is slightly above the cut-off frequency of mode 4. The contribution of mode 4 in the upper subplot of Fig. 9 is accordingly weak and mainly observed at short range.

The interference patterns can be better understood by inspection of Fig. 10, that shows results at a frequency of 122 kHz for the two additional source depths:

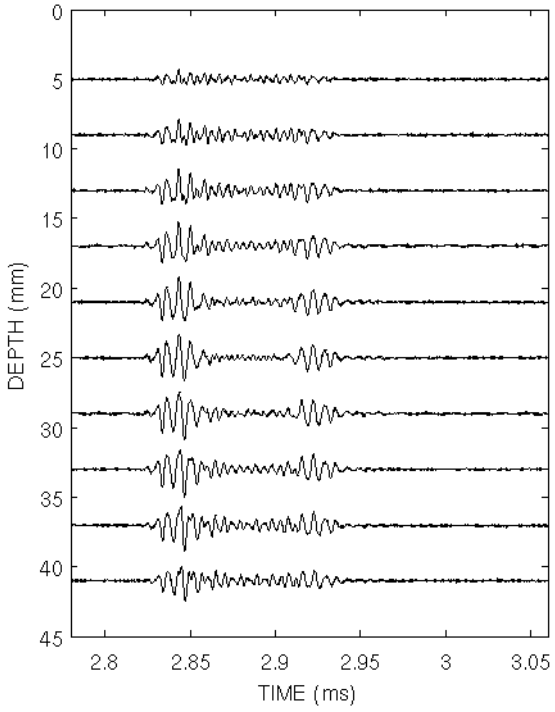

Figure 8: Stacked time series *vs.* receiver depth at a source/receiver range of 4100 mm. We identify two arrivals of mode 1. All other modes have been shadowed.

SD = 19 mm where mode 3 is weakly excited, and at SD = 26.9 mm where modes 2 and 4 are not excited. In

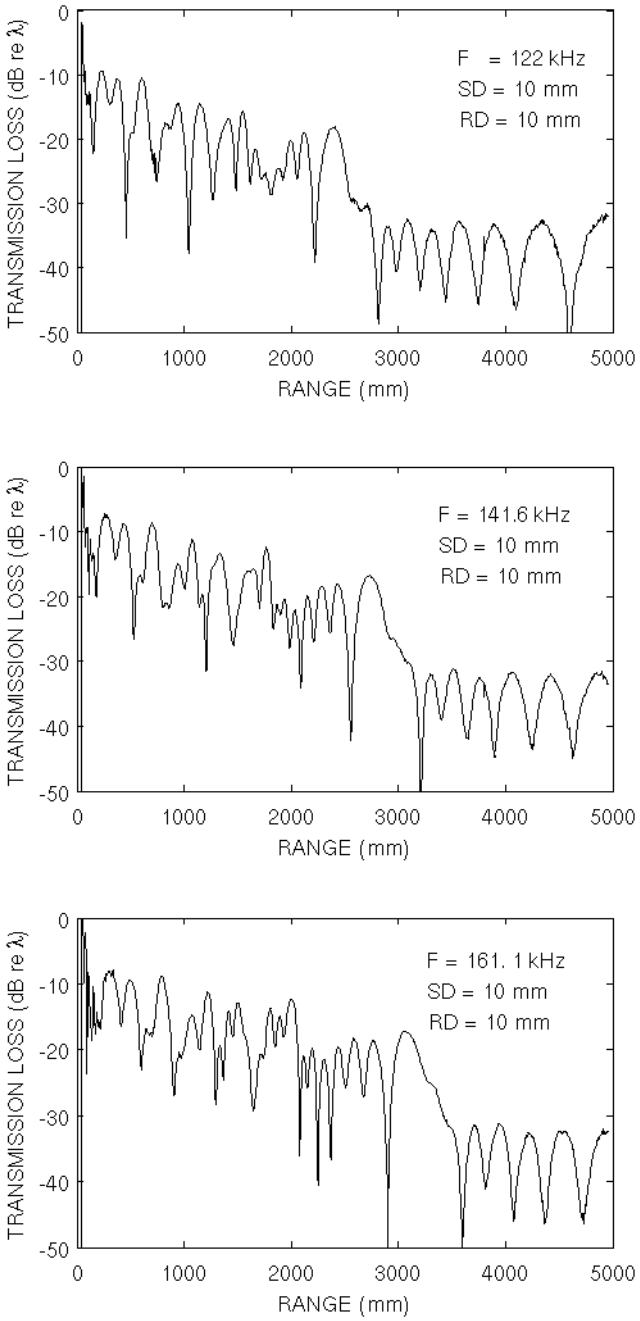

Figure 9: Transmission loss *vs.* range extracted from time-domain data at three different frequencies: 122 kHz (upper subplot), 141.6 kHz (middle subplot), and 161.1 kHz (lower subplot).

the upper subplot we see that up to $r \approx 900$ mm mode 4 is present. Then up to $r \approx 1900$ mm we see typical interference patterns between mode 1 and mode 2 with a slight perturbation due to a very likely weak contribution of mode 3. Inspecting now the lower subplot where modes 2 and 4 are poorly excited, we recognize typical interference patterns between modes 1 and 3 up to $r \approx 1700$ mm. Besides, the increase in the transmission loss curve around $r \approx 1500$ mm corresponds to multiple arrivals of mode 3. Beyond $r \approx 1700$ mm mode 3 is entirely shadowed, *i.e.* completely refracted out of the vertical plane in the cross-slope direction. Hence, from $r \approx 1700$ mm only mode 1 is present, and beyond $r \approx 2100$ mm we get an interference pattern attributed

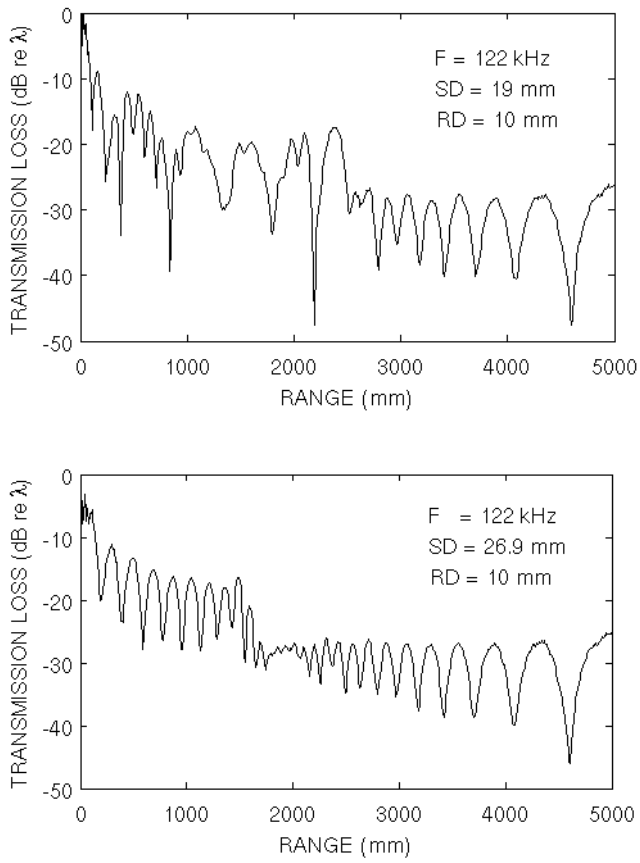

Figure 10: Transmission loss *vs.* at 122-kHz frequency for two additional source depths: SD = 19 mm (upper subplot) and SD = 26.9 mm (lower subplot).

to two arrivals of mode 1. Looking back at the upper subplot of Fig. 10 we conclude that the pattern between $r \approx 1900$ mm and $r \approx 2100$ mm is that of the interference between mode 1 and the two arrivals of mode 2. Then, up to $r \approx 2500$ mm we get in addition a second arrival of mode 1. Beyond this range, mode 2 is being shadowed and mode 1 interferes with itself only. The lobes within this pattern are strectched with increasing range. After some range, mode 1 would be shadowed as well, leading to no acoustic energy from the initial pulse in the cross-slope direction. The available tank length did not permit us to observe it. It was however observed during other measurement campaigns with smaller water depth values.

4 Conclusion and discussion

Additional measurement campaigns were plannified to obtain high quality experimental data of acoustic propagation in the cross-slope direction over a wedge-shaped oceanic bottom. These followed a calibration phase in a range-independent environment and preliminary tests in the wedge-like environment to gain good understanding of the shallow-water tank behavior. The data are intended to be used in model-based inversion techniques such as matched-field processing (MFP) with replica provided by a fully 3-D PE code.

The main objective in the inversion procedure is to recover some geometrical characteristics of the waveg-

uide (*e.g.* the slope of the tilted bottom) in addition to geoacoustic parameters. Current work is focused on the sensitivity study of generalized Bartlett processors commonly used in MFP, with respect to dominant parameters such as the slope of the bottom, the water depth at the source, and the bottom sound speed. During the experiment, an effort was made to record the signals in a fine spatial grid in order to allow testing several (virtual) array geometries, *e.g.* horizontal arrays, vertical arrays, or L-shaped arrays at several locations within the vertical plane in the cross-slope direction. Results of the ongoing work will be presented during the oral presentation. Future work will focus on the issue of the considerably increased CPU time needed for the inversion procedure. Indeed, the generation of replica vectors with a fully 3-D code is several orders more CPU time consuming compared to a 2-D model traditionally used in MFP over the last decades. Global optimization techniques will be considered, such as genetic algorithms, but still the CPU time will remain higher. However, most of the parameters of the waveguide are known with sufficient accuracy to meet our needs, with the exception of the bottom sound speed and the water depth at the source. This point was discussed in [10]. Hence, only a few number of parameters need to be included in the inversion procedure, thus allowing to perform the inversion in more realistic CPU times.

References

[1] J. M. Collis, W. L. Siegmann, M. D. Collins, H. J. Simpson, R. J. Soukup, "Comparison of simulations and data from a seismo-acoustic tank experiment", *J. Acoust. Soc. Am.* **122**, 1987–1993 (2007).

[2] M. A. Ainslie, L. S. Wang, C. H. Harrison, N. G. Pace, "Numerical and laboratory modeling of propagation over troughs and ridges", *J. Acoust. Soc. Am.* **94**, 2287–2295 (1993).

[3] S. A. L. Glegg, G. B. Deane, I. G. House, "Comparison between theory and model scale measurements of three-dimensional sound propagation in a shear supporting penetrable wedge", *J. Acoust. Soc. Am.* **94**, 2334–2342 (1993).

[4] S. A. L. Glegg, A. J. Hundley, J. M. Riley, J. Yuan, H. Uberall, "Laboratory scale measurements and numerical predictions of underwater sound propagation over a sediment layer", *J. Acoust. Soc. Am.* **92**, 1624–1630 (1992).

[5] L. S. Wang, N. G. Pace, M. A. Ainslie, and C. H. Harrison, "Experimental study of sound propagation in modelled shallow-water environments", *Ultrasonics* **32**, 141–147 (1994).

[6] J.-P. Sessarego, "Scaled models for underwater acoustics and geotechnics applications", *In Proceedings of the 6th European Conference on Underwater Acoustics* (Gdansk, Poland, 24-27 June 2002), Editor A. Stepnowski, Co-editors: R. Salamon and A. Partyka (European Commission 2002, ISBN 83-907591-8-7), pp. 359–364.

[7] F. Sturm, J.-P. Sessarego, P. Sanchez, "Comparison of Parabolic Equation based Codes with Tank Experiments for Shallow Water Environments", *In Proceedings of the 8th European Conference on Underwater Acoustics* (Carvoeiro, Portugal, 12-15 June 2006), edited by S. M. Jesus and O. C. Rodriguez (ISBN 989-95068-0-X), Vol. 1, pp. 427-432.

[8] P. Papadakis, M. Taroudakis, P. Sanchez, J.-P. Sessagrego, "Time and frequency measurements using scaled laboratory experiments of shallow water acoustic propagation", *In Proceedings of the 8th European Conference on Underwater Acoustics* (Carvoeiro, Portugal, 12-15 June 2006), edited by S. M. Jesus and O. C. Rodriguez (ISBN 989-95068-0-X), Vol. 1, pp. 453–458.

[9] F. Sturm, J.-P. Sessarego, D. Ferrand, "Laboratory scale measurements of across-slope sound propagation over a wedge-shaped bottom", *In Proceedings of the 2nd International Conference & Exhibition on Underwater Acoustic Measurements: Technologies & Results* (FORTH, Heraklion, Crete, Greece, 25-29 June 2007), edited by John S. Papadakis and Leif Bjorno (ISBN 978-960-88702-9-1), Vol. III, pp. 1151-1156.

[10] A. Korakas, F. Sturm, J.-P. Sessarego, D. Ferrand, "Investigation of pulse propagation in shallow water laboratory experiments and comparison with numerical simulations", *In Proceedings of the 2nd International Conference & Exhibition on Underwater Acoustic Measurements: Technologies & Results* (FORTH, Heraklion, Crete, Greece, 25-29 June 2007), edited by John S. Papadakis and Leif Bjorno (ISBN 978-960-88702-9-1), Vol. III, pp. 1123–1128.

[11] C. H. Harrison, "Acoustic shadow zones in the horizontal plane", *J. Acoust. Soc. Am.* **65**, 56–61 (1979).

[12] F. Sturm, "Numerical study of broadband sound pulse propagation in three-dimensional oceanic waveguides", *J. Acoust Soc. Am.* **117**, 1058–1079 (2005).

[13] K. Castor, F. Sturm, "Investigation of 3-D acoustical effects using a multiprocessing parabolic equation based algorithm", to appear in *Journal of Computational Acoustics*.

[14] W. S. Burdic, *Underwater acoustic system analysis*, Prentice Hall (New Jersey, 1991).

[15] N. Bilaniuk, G.S.K. Wong, "Speed of sound in pure water as a function of temperature", *J. Acoust. Soc. Am.* **93**, 1609–1612 (1993).